Mem. S.A.It. Vol. 84, 1053

Memorie della

Atmospheres from very low-mass stars to extrasolar planets

F. Allard, D. Homeier, and B. Freytag

CRAL, UMR 5574, CNRS, Université de Lyon, École Normale Supérieure de Lyon, 46 Allée d'Italie, F-69364 Lyon Cedex 07, France, e-mail: fallard@ens-lyon.fr

Abstract. Within the next few years, several instruments aiming at imaging extrasolar planets will see first light. In parallel, low mass planets are being searched around red dwarfs which offer more favorable conditions, both for radial velocity detection and transit studies, than solar-type stars. We review recent advancements in modeling the stellar to substellar transition. The revised solar oxygen abundances and cloud models allow to reproduce the photometric and spectroscopic properties of this transition to a degree never achieved before, but problems remain in the important M-L transition characteristic of the $T_{\rm eff}$ range of characterisable exoplanets.

Key words. Stars: atmospheres – M dwarfs – Brown Dwarfs – Extrasolar Planets

1. Introduction

Since spectroscopic observations of very low mass stars (late 80s), brown dwarfs (mid 90s), and extrasolar planets (mid 2000s) are available, one of the most important challenges in modeling their atmospheres and spectroscopic properties lies in high temperature molecular opacities and cloud formation. K dwarfs show the onset of formation metal hydrides (starting around $T_{\rm eff} \sim 4500$ K), TiO and CO (below $T_{\rm eff} \sim 4000$ K), while water vapor forms in early M dwarfs ($T_{\rm eff} \sim 3900 - 2000$ K), and methane, ammonia and carbon dioxide are detected in late-type brown dwarfs ($T_{\rm eff} \sim 300-1600$ K) and in extrasolar giant planets. Cloud formation is also an important factor in the detectability of biosignatures, and for the habitability of exoplanets (Paillet et al. 2005; Kasting 2001)

Send offprint requests to: F. Allard

Extrasolar planets for which we can currently characterize their atmospheres are either those observed by transit ($T_{\rm eff} \sim 1000-2000$ K depending on their radius relative to that of the central star) or by imaging (young planets of $T_{\rm eff} \sim 500 - 2000$ K depending on their mass and age). Several infrared integral field spectrographs combined with coronagraph and adaptive optic instruments are coming online before 2013 (SPHERE at the VLT, the Gemini Planet Imager at Gemini south, Project1640 at Mount Palomar, etc.). The E-ELT 39 m telescope in Chile due around 2020 will also be ideally suited for planet imaging.

M dwarfs are the most numerous stars, constituting 70% of the stellar budget of the Galaxy (Chabrier 2003, 2005), and 1281 brown dwarfs[1] and 891 planets[2] are currently

[1] according to http://DwarfArchives.org
[2] according to http://Exoplanet.eu

known despite their faintness in the solar neighborhood vicinity. Single very low mass (VLM) stars and brown dwarfs are therefore more directly observable and characterizable then exoplanets. They represent, beyond their own importance, a wonderful testbed for the understanding of exo-planetary atmospheric properties together with solar system studies.

2. Model construction

The modeling of the atmospheres of VLMs has evolved (as here illustrated with the development of the PHOENIX atmosphere code) with the extension of computing capacities from an analytical treatment of the transfer equation using moments of the radiation field (Allard 1990), to a line-by-line opacity sampling in spherical symmetry (Allard et al. 1994, 1997; Hauschildt et al. 1999) and more recently to 3D radiation transfer (Seelmann et al. 2010).

To illustrate the various assumptions made by constructing model atmospheres, let us begin with the description of the equations of ideal magnetohydrodynamics (MHD) — adapted here for the stellar case by specifying the role of gravity, radiative transfer, and energy transport — which are themselves a special case (no resistivity) of the more general equations (see for example Landau & Lifshitz 1960). These are written in the compact vector notation as:

$$\begin{aligned}
&\frac{\partial \rho}{\partial t} + \nabla\cdot(\rho\mathbf{v}) = 0 \ , \\
&\frac{\partial \rho\mathbf{v}}{\partial t} + \nabla\cdot(\rho\mathbf{v}\mathbf{v} + (P + \frac{1}{2}\mathbf{B}\cdot\mathbf{B})\mathbf{I} - \mathbf{B}\mathbf{B}) = \rho\mathbf{g}, \\
&\frac{\partial \mathbf{B}}{\partial t} + \nabla\cdot(\mathbf{v}\mathbf{B} - \mathbf{B}\mathbf{v}) = 0 \ , \\
&\frac{\partial \rho e_{\rm t}}{\partial t} + \nabla\cdot((\rho e_{\rm t} + P + \frac{1}{2}\mathbf{B}\cdot\mathbf{B})\mathbf{v} \\
&\qquad - (\mathbf{v}\cdot\mathbf{B})\mathbf{B} + \mathbf{F}_{\rm rad}) = 0 \ .
\end{aligned} \tag{1}$$

The vectors are noted with boldface characters, while scalars are not. For example, P is the gas pressure, ρ the mass density, $\mathbf{g}$ the gravity, and $\mathbf{v}$ is the gas velocity at each point in space. $\mathbf{B}$ is the magnetic field vector, where the units were chosen such that the magnetic permeability μ is equal to one. $\mathbf{I}$ is the identity matrix and $\mathbf{a}\cdot\mathbf{b} = \sum_k a_k b_k$ the scalar product of the two vectors $\mathbf{a}$ and $\mathbf{b}$. The dyadic tensor product of two vectors $\mathbf{a}$ and $\mathbf{b}$ is the tensor $\mathbf{ab} = \mathbf{C}$ with elements $c_{mn} = a_m b_n$ and the nth component of the divergence of the tensor $\mathbf{C}$ is $(\nabla\cdot\mathbf{C})_n = \sum_m \partial c_{mn}/\partial x_m$. In this case, the total energy is given by

$$\rho e_{\rm t} = \rho e_{\rm i} + \rho\frac{1}{2}\mathbf{v}\cdot\mathbf{v} + \frac{1}{2}\mathbf{B}\cdot\mathbf{B} + \rho\Phi \ , \tag{2}$$

where $e_{\rm i}$ is again the internal energy per unit mass, and Φ the gravitational potential. The additional constraint for the absence of magnetic monopoles,

$$\nabla\cdot\mathbf{B} = 0 \ , \tag{3}$$

must also be fulfilled.

The first, third, and last equations in Eq. 1 correspond to the mass, magnetic field, and energy conservation, while the second equation is the budget of forces acting on the gas. In the case of stellar astrophysics, gravitational acceleration is an important source term, while the radiative flux participates in the energy budget. Further assumptions are made in the numerical solution of these equations to address different astrophysical problems in very different regimes. The chromospheres correspond to a regime of high Mach numbers and strong magnetic fields where ionized gas has to follow the magnetic field lines, and where the radiative transfer must be solved for the case of a non-ideal gas.The photospheric convection simulations correspond to a regime where the thermal and convective turnover timescales are comparable i.e. Mach numbers are around 1, and the non-local radiative transfer must be solved, often for an ideal gas. And the interior convection and/or dynamo simulations correspond to a regime where the thermal timescale is much larger then the turnover timescale, which in turn is much larger then the acoustic timescale. The radiative flux can be estimated by the diffusion approximation, and the magnetic field lines are dragged by the ionized gas.

The classical approach for interior and atmosphere models consists in simplifying the problem for a gain of computing efficiency, neglecting the magnetic field, convective and/or rotational motions and other multi-

dimensional aspects of the problem, and assuming that the averaged properties of stars can be approximated by modeling their properties radially (uni-dimensionally) and statically. We also assume that the atmosphere does neither create nor destroy the radiation emitted through it. Neglecting motions in modeling the photospheres of VLM stars, brown dwarfs, and planets is acceptable since the convective velocity fluctuation effects on line broadening is hidden by the strong van der Waals broadening prevailing in these atmospheres. But this is not the case of the impact of the velocity fields on the cloud formation and wind processes (see section 3 below). In this case, equation 1 reduces to the so-called hydrostatic equation and constant flux approximation for the radial or z direction used in classical models:

$$\begin{aligned} \frac{\partial P}{\partial r} &= -\rho g \ , \\ \frac{\partial F_{\rm rad}}{\partial r} &= \frac{\partial(\int F_\lambda \, {\rm d}\lambda)}{\partial r} = 0 \ . \end{aligned} \tag{4}$$

This allows computing the interior evolutive properties of stars throughout the Hertzsprung-Russell diagram, and to solve the radiative transfer in the atmosphere for a much larger number of wavelengths (line-by-line or opacity sampling) or wavelength bins (Opacity Distribution Function or ODF, K-Coefficient) compared to R(M)HD simulations. Classical model atmospheres impose therefore the independent parameter $F_{\rm rad}$ ($= \sigma\ T_{\rm eff}$, where σ is the Stefan-Boltzmann constant) and compute F_λ so that, after model convergence, the target $F_{\rm rad}$ is reached. Other independent parameters are the surface gravity g and the abundances of the elements ϵ_i. This makes it possible to create extensive databases of synthetic spectra and photometry that provide the basis for the interpretation of stellar observations.

All the model atmospheres compared in this review are classical models in this sense, and differ mainly in the completeness and accuracy of their opacity database including their cloud model assumptions), and the assumed solar abundances used for the particular grid shown. They must resolve the radiative transfer for the entire spectral energy distribution (as can be seen from Eq. 4) with a good enough spectral resolution to account for all cooling and heating processes.

The PHOENIX code (Allard et al. 1994, 2012) distinguishes itself by computing the opacities during the model execution (or on-the-fly). This involves computing the opacities for billions of atomic and molecular transitions on-the-fly, though with a selection of the most important lines. This different approach makes PHOENIX much slower then former codes, but allows to take into account more consistently important physical phenomena, such as those involving a modification of local elemental abundances along the atmospheric structure (e.g. non-LTE, photoionisation, diffusion and cloud formation).

3. Mixing

Stars becomes fully convective throughout their interior and convection reaches furthest out in the optically thin regions of the photosphere in M3 and later dwarfs with $T_{\rm eff}$ below 3200 K (Allard 1990; Chabrier & Baraffe 2000). In most model atmospheres discussed in this review paper, the convective energy transfer is treated using the Mixing Length Theory (or MLT, see Kippenhahn & Weigert 1994), using at best a unique fixed value of the mixing length of 1.0 (1.25 for the ATLAS9 models, 1.5 for the MARCS models, etc). However, since convection becomes efficient in M dwarfs, the precise value of the mixing length matters only for the deep atmospheric structure and as a surface boundary condition for interior models.

Ludwig et al. (2002, 2006) have been able to compare the PHOENIX thermal structure obtained using the MLT with that of RHD simulations. They showed that the MLT could reproduce adequately (except for the overshoot region) the horizontally averaged thermal structure of the hydro simulations when using an adequate value of the mixing length parameter. This value has been estimated for M dwarfs to vary with a gravity from $\alpha{=}l/H_p{=}1.8$ to 2.2 (2.5 to 3.0 for the photosphere). The BT-Settl models use the mass and gravity dependent prescription of Ludwig et al. (1999) for hotter stars, together with an average (2.0) of

the values derived for M dwarfs by Ludwig et al. (2002, 2006). They also use the microturbulence velocities from the RHD simulations (Freytag et al. 2010), and the velocity field from RHD simulations from Ludwig et al. (2006) and Freytag et al. (2010) to calibrate the scale height of overshoot, which becomes important in forming thick clouds in L dwarfs but is negligible for the SED of VLMs and brown dwarfs otherwise.

3.1. The revision of solar abundances

Model atmospheres assume scaled solar abundances for all elements relative to hydrogen. Additionally, some enrichment of α-process elements (C, O, Ne, Mg, Si, S, Ar, Ca, and Ti) resulting from a "pollution" of the star-forming gas by the explosion of a supernova is appropriate in the case of metal-poor subdwarfs of the Galactic thick disk, halo, and globular clusters, and the stars towards the galactic center (Gaidos et al. 2009).

Since the overall SED of late K dwarfs, M dwarfs, brown dwarfs, and exoplanets is governed by oxygen compounds (TiO, VO in the optical and water vapor and CO in the infrared), the elemental oxygen abundance is of major importance. Important revisions have been made to the solar abundances based on radiation hydrodynamical simulations of the solar photosphere, and to improvements in the detailed line profile analysis. Indeed, two separate groups using independent RHD and spectral synthesis codes (Asplund et al. 2009; Caffau et al. 2011) obtain an oxygen reduction of 34% and 22% respectively) compared to the abundances of Grevesse et al. (1993) previously used in the NextGen and AMES-Cond/Dusty models.

Figs. 8 and 9 of Rajpurohit et al. (2012) shows an example of these effects, where several models are compared to the optical to infrared SED of the M5.5, M9.5, and L0 dwarfs of the LHS 1070 system. The BT-Settl model by Allard et al. (2012) is based on the Caffau et al. (2011) solar abundance values, while DRIFT models by Helling et al. (2008b) use the Grevesse et al. (1993) solar abundances, and the MARCS model by Gustafsson et al. (2008) uses the values of Grevesse et al. (2007, 39%). The MARCS model show a systematic near-infrared flux excess, compared both to observations and the other models, which is probably caused by the much lower oxygen abundance values of Grevesse et al. (2007). The oxygen abundances sensitivity of TiO bands is expressed as a reduced line blanketing effect at longer wavelengths, participating in the water vapor profile changes (Allard et al. 2000).

The influence of the solar oxygen abundance can also be clearly seen in Fig. 1 which compares the Casagrande et al. (2008) $T_{\rm eff}$ and metallicity estimates with the Baraffe et al. (1998) NextGen isochrones (assuming an age of 5 Gyrs) using model atmospheres from various authors. The oxygen abundance effects are particularly highlighted by comparing the BT-Settl model based on the Caffau et al. (2011) values with models based on earlier solar abundance values. This is the case of the AMES-Cond/Dusty and BT-NextGen models which are based on the Grevesse et al. (1993) solar abundances. On can see that the higher oxygen abundance causes models to appear too blue by as much as 0.75 mag compared to models based on the Caffau et al. (2011) values. The MARCS models (Gustafsson et al. 2008) based on the Grevesse et al. (2007) values show on the contrary a systematically increasing excess in $J-K_s$ with decreasing $T_{\rm eff}$. The models are most sensitive on the solar oxygen abundances for M dwarfs around 3300 K, i.e. at the onset of water vapor formation.

By comparing the BT-Settl 2012 isochrone, computed using the Caffau et al. (2011) solar abundances, to the BT-Dusty isochrone computed using the Asplund et al. (2009) values, we note that the remaining uncertainties tied to the solar abundance determination correspond only to 0.02 mag in the $J-K_s$ color. Rajpurohit et al. (2013) have compared the BT-Settl 2012 models to the observed optical spectra and colors of M dwarfs from M0 to M9, and found an excellent agreement of the models with observations except in the $T_{\rm eff}$ = 2000 − 2500 K regime affected by the onset of important cloud formation (see section 4).

The NextGen model by Hauschildt et al. (1999) dates too far back and suffers from too

much opacity differences (incompleteness essentially) to participate in this illustration. In fact, this plot helps to conclude that using the NextGen models caused a systematic overestimation of $T_{\rm eff}$ for VLM stars. It is interesting to note that all models appear too red in the K dwarf range above 4000 K. This may be due to an under representation of the K dwarfs in this diagram. The unified cloud model (hereafter UCM) by Tsuji (2002) show a completely different behavior in this diagram, sharing the colors of NextGen or even MARCS models at 4000 K, but diverging towards the BT-Settl colors at 3500 K to finally cross-over to bluer colors as dust begin to form and affect the SED below 2600 K.

The various model atmospheres have not been used as surface boundary condition to interior and evolution calculations, and simply provide the synthetic color tables interpolated on the published theoretical isochrones (Baraffe et al. 1998). Even if the atmospheres partly control the cooling and evolution of M dwarfs (Chabrier & Baraffe 1997), differences introduced in the surface boundary conditions by changes in the model atmosphere composition have negligible effect.

In the substellar regime, the composition of brown dwarfs varies rapidly with decreasing $T_{\rm eff}$, and the variation is responsible for the immense change in their SED across the very narrow $T_{\rm eff}$ regime of the M-L-T spectral transition. If water vapor opacities only became recently reliable (Allard et al. 2012), this is not the case of the more complex methane molecule which is so important in brown dwarfs, and planetary atmospheres. The ExoMol Project supported by an European Research Council grant to Jonathan Tennyson (University College London) will allow important advances on these fronts in the coming years. New ammonia line lists are already available through this project (Yurchenko et al. 2011) and from the NASA-Ames group (Huang et al. 2011a,b).

4. Cloud formation

One of the most important challenges in modeling these atmospheres is the formation of clouds. Tsuji et al. (1996) had identified dust formation by recognizing the condensation temperatures of hot dust grains (enstatite, forsterite, corundum: $MgSiO_3$, Mg_2SiO_4, and Al_2O_3 crystals) to occur in the line-forming layers ($\tau \approx 10^{-4} - 10^{-2}$) of their models. The onset of this phase transition occurs in M dwarfs below $T_{\rm eff} = 3000$ K, but the cloud layers are too sparse and optically thin to affect the SED above $T_{\rm eff} = 2600$ K. The cloud composition, according to equilibrium chemistry, is going from zirconium oxide (ZrO_2), refractory ceramics (perovskite and corundum; $CaTiO_3$, Al_2O_3), silicates (e.g. forsterite; Mg_2SiO_4), to salts (CsCl, RbCl, NaCl), and finally to ices (H_2O, NH_3, NH_4SH) as brown dwarfs cool down over time from M through L, T, and Y spectral types (Allard et al. 2001; Lodders & Fegley 2006). This crystal formation causes the weakening and vanishing of TiO and VO molecular bands (via $CaTiO_3$, TiO_2, and VO_2 grains) from the optical spectra of late M and L dwarfs, revealing CrH and FeH bands otherwise hidden by the molecular pseudo-continuum, and the resonance doublets of alkali transitions which are only condensing onto salts in late-T dwarfs. The scattering effects of this fine dust is Rayleigh scattering which provides veiling to the optical SED, while the greenhouse effect due to the dust cloud causes their infrared colors to become extremely red compared to those of hotter dwarfs. The upper atmosphere, above the cloud layers, is depleted from condensible material and significantly cooled down by the reduced or missing pseudo-continuum opacities.

One common approach has been to explore the limiting properties of cloud formation. One limit is the case where sedimentation or gravitational settling is assumed to be fully efficient. This is the case of the Case B model of Tsuji (2002), the AMES-Cond model of Allard et al. (2001), the Clear model of (Burgasser et al. 2002), and the Clear model of Burrows et al. (2006). The other limit is the case where gravitational settling is assumed inefficient and dust, often only forsterite, forms in equilibrium with the gas phase. This is the case of of the Case A model of Tsuji (2002), the AMES-Dusty models of Allard et al. (2001), the BT-Dusty mod-

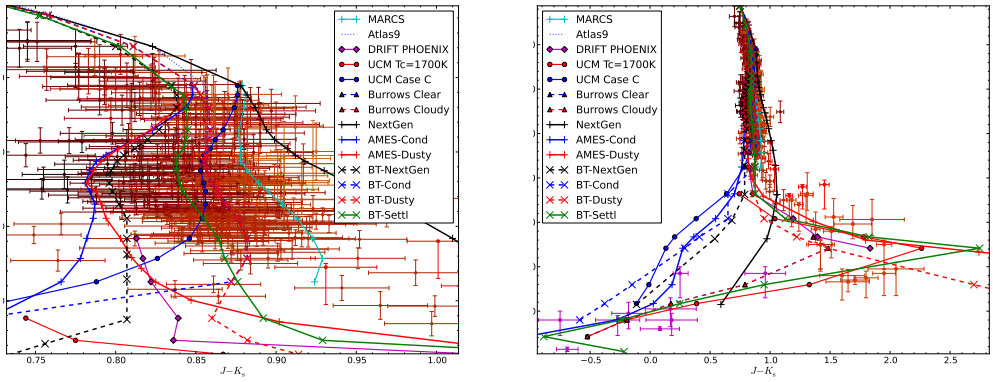

Fig. 1. Estimated $T_{\rm eff}$ and metallicity (lighter to darker tones) for M dwarfs by Casagrande et al. (2008) on the left, and brown dwarfs by Golimowski et al. (2004) and Vrba et al. (2004) on the right are compared to the NextGen isochrones for 5 Gyrs Baraffe et al. (1998) using model atmospheres by various authors: MARCS by Gustafsson et al. (2008), ATLAS9 by Castelli & Kurucz (2004), DRIFT-PHOENIX by Helling et al. (2008b), UCM by Tsuji (2002), Clear/Cloudy by Burrows et al. (2006), NextGen by Hauschildt et al. (1999), AMES-Cond/Dusty by Allard et al. (2001), and the BT models by Allard et al. (2012). The region below 2900 K is dominated by dust formation. The dust free models occupy the blue part of the diagram and only at best explain T dwarf colors, while the Dusty and DRIFT models explain at best L dwarfs, becoming only redder with decreasing $T_{\rm eff}$. The BT-Settl, Cloudy and UCM $T_{\rm crit}$ = 1700 K models describe a complete transition to the red in the L dwarf regime before turning to the blue into the T dwarf regime. The Cloudy model however does not explain the reddest L dwarfs.

els of Allard et al. (2012), the Dusty model of Burgasser et al. (2002), and the Cloudy model of Burrows et al. (2006). To these two limiting cases we can add a third case also explored by several, which is the case where condensation is not efficient and the phase transition does not take place. This is the case of the NextGen models of Hauschildt et al. (1999), of the BT-NextGen models of Allard et al. (2012), and the Case B models of (Tsuji 2002, not shown).

The purpose of a cloud model is to go beyond these limiting cases and define the number density and size distribution of condensates as a function of depth in the atmosphere, and as a function of the atmospheric parameters. Helling et al. (2008a) have compared different cloud models and their impact on model atmospheres of M and brown dwarfs. Most cloud models define the cloud base as the evaporation layer provided by equilibrium chemistry. In the unified cloud model of Tsuji (2002) and Tsuji et al. (2004) a parametrization of the radial location of the cloud top by way of an adjustable parameter $T_{\rm crit}$ was used. This choice permits to parametrize the cloud extension effects on the spectra of these objects without resolving the cloud model equations. In principle, this approach does not allow to reproduce the stellar-substellar transition with a unique value of $T_{\rm crit}$ since the cloud extension depends on $T_{\rm eff}$. Indeed, the transparent T dwarf atmospheres can only exist if the forsterite cloud layers retract below the line-forming regions in those atmospheres.

Ackerman & Marley (2001) have solved the particle diffusion problem assuming a parametrized sedimentation efficiency $f_{\rm sed}$ (constant through the atmosphere) and a mixing assumed constant and fixed to its maximum value (maximum of the inner convection zone). Burgasser et al. (2002) and Saumon & Marley (2008) found that their so-called Cloudy models could not produce the M-L-T spectral transition with a single value of $f_{\rm sed}$. This conclusion prompted them to propose a patchy cloud model Marley et al. (2010).

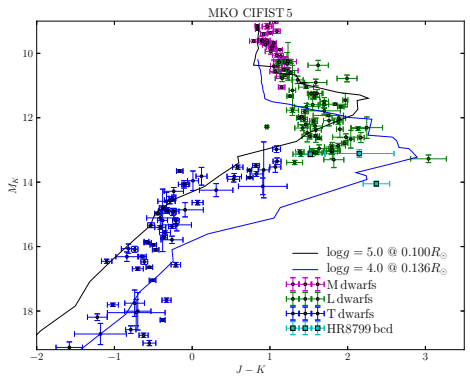

Fig. 2. Color-magnitude diagram of late-type dwarfs (MKO system, Dupuy & Liu 2012) and directly imaged HR8799 exoplanets (Marois et al. 2008) compared to two isogravity tracks of the BT-Settl models, representative of old and young brown dwarfs or planetary mass objects. The models span most of the observed locus of L and early T dwarfs and show the transition from cloudy to (nearly) clear atmospheres around $T_{\rm eff}$ = 1000 − 1500 K, at practically constant J-band luminosity. Late T dwarfs show systematically redder NIR colors possibly explained by sulfide and chloride clouds forming at lower temperatures (Morley et al. 2012).

Allard et al. (2003, 2012) have developed PHOENIX version 15.05 using the index of refraction of 55 condensible species, and a slightly modified version of the Rossow cloud model obtained by ignoring the coalescence and coagulation, and computing the supersaturation consistently. Their density and grain size distribution with depth in the atmosphere is obtained by comparing the timescales for nucleation, condensation, gravitational settling or sedimentation, and mixing derived from the MLT for the convective mixing in the convection zones, exponential overshoot according to Ludwig et al. (2002, 2006), and from gravity waves according to Freytag et al. (2010). The cloud model is solved layer by layer inside out (bottom up) to account for the sequence of grain species formation as a function of cooling of the gas. Among the most important species forming in the BT-Settl model are ZrO_2, Al_2O_3, $CaTiO_3$, $Ca_2Al_2SiO_7$, $MgAl_2O_4$, Ti_2O_3, Ti_4O_7, $Ca_2MgSi_2O_7$, $CaMgSi_2O_6$, $CaSiO_3$, Fe, Mg_2SiO_4, $MgSiO_3$, Ca_2SiO_4, $MgTiO_3$, $MgTi_2O_5$, $Al_2Si_2O_{13}$, VO, V_2O_3, and Ni. At each step, the gas phase is adjusted for the depletion caused by grain formation and sedimentation. The grain sizes (a unique maximum value per atmospheric layer) are determined by the comparison of the different timescales and thus varies with depth to reach a few times the interstellar values (used in the dusty limiting case models) at the cloud base for the effective temperatures discussed in this paper. While the BT-Settl model assumes dirty spherical grains in the timescales equations to calculate the growth and settling of the grains, it only sums the opacity contributions of each species in each layer as for an ensemble of pure spherical grains.

Helling et al. (2008b) and Witte et al. (2009) modified the PHOENIX code to compute the DRIFT-PHOENIX models, considering the nucleation of only seven of the most important solids (TiO_2, Al_2O_3, Fe, SiO_2, MgO, $MgSiO_3$, Mg_2SiO_4) made of six different elements. The cloud model is based on resolving the moment equations for the dust density accounting for nucleation on seed particles and their subsequent growth or evaporation, solving from top to bottom of the atmosphere. This model assumes dirty grains mixed according to the composition of each atmospheric layer. It uses composite optical constants resulting in absorption and scattering properties of the grains that are therefore different than those of the BT-Settl models, possibly producing more opaque clouds. However, since the opacities are dominated by atomic and molecular opacities over most of the spectral distribution in this spectral type range, the impact of those differences are difficult to identify. The largest differences between the BT-Dusty, BT-Settl and DRIFT models are the differences in the local number density, the size of dust grains, as well as their mean composition, which are the direct results of the cloud model approach.

The models using the limiting cases of maximum dust content describe adequately (given the prevailing uncertainties) the infrared colors of L dwarfs. The cloud-free limiting case models, on the other hand, allow to reproduce to some degree the colors of T

dwarfs. But pure equilibrium chemistry models without parametrization of the cloud extension in the atmosphere cannot reproduce the observed behaviour of the M-L-T transition, the dusty models only becoming redder and dustier with decreasing $T_{\rm eff}$, while dust-free models miss completely the reddening due to the dust greenhouse effects in the L dwarf regime. Fig. 1 shows this situation compared with the effective temperatures estimates obtained by integration of the observed SED (Golimowski et al. 2004; Vrba et al. 2004). One can see that the late-type M and early-type L dwarfs behave as if dust is formed nearly in equilibrium with the gas phase with extremely red colors in some agreement with the AMES-Dusty models. The BT-Settl models reproduce the main sequence down to the L-type brown dwarf regime, before turning to the blue in the late-L and T dwarf regime as a result of the onset of methane formation in the K_s bandpass. The BT-Settl models succeed as good as the limiting case AMES-Dusty, BT-Dusty, and UCM $T_{\rm crit}$ = 1700 K at explaining the reddest colors of L dwarfs (assuming an age of 5 Gyrs). The fact that a UCM model with $T_{\rm crit}$ value of 1700 K succeeds rather well in reproducing the L-T transition suggest that the cloud extension is somewhat constant through that transition. The DRIFT models, on the other hand, reach slightly less to the red and do not extend low enough in temperature to explain the L-T transition. The M-L transition is not reproduced by any models where the BT-Settl models shows a J-band flux excess. This suggests that an additional element neglected thus far is at play, such as larger maybe porous grains. Indeed, all models assume thus far spherical and non-porous grains. The choice of solar abundances and the completeness of the opacity databases used is also important.

5. Conclusions

We have compared the behavior of the recently published model atmospheres from various authors across the M-L-T spectral transition from M dwarfs through L type and T type brown dwarfs and confronted them to constraints. If the onset of dust formation is occurring below $T_{\rm eff}$ = 2900 K, the greenhouse effects of silicate dust cloud formation impact strongly ($J - K_s < 2.0$) the near-infrared SED of late-M and L-type atmospheres with 1300 < $T_{\rm eff}$ < 2600 K. The BT-Settl models by Allard et al. (2012) are the only models to span the entire regime from stars to Y type brown dwarfs. In the M dwarf range, the results appear to favor the BT-Settl models based on the Caffau et al. (2011) solar abundances versus MARCS and ATLAS 9 models based on other values. In the brown dwarf (and planetary) regime, on the other hand, the unified cloud model by Tsuji (2002) succeeds extremely well in reproducing the constraints, while the BT-Settl models also show a plausible transition. However, no models succeed in reproducing the M-L transition between 2500 and 2000 K. The BT-Settl models also reproduce the redder infrared colors of young planets directly observable by imaging as an effect of their lower surface gravities.

Acknowledgements. The research leading to these results has received funding from the French "Agence Nationale de la Recherche" (ANR), the "Programme National de Physique Stellaire" (PNPS) of CNRS (INSU), and the European Research Council under the European Community's Seventh Framework Programme (FP7/2007-2013 Grant Agreement no. 247060).

References

Ackerman, A. S., & Marley, M. S. 2001, ApJ, 556, 872
Allard, F. 1990, PhD thesis, Ruprecht Karls Univ. Heidelberg
Allard, F., et al. 2001, ApJ, 556, 357
Allard, F., et al. 2003, in Brown Dwarfs, ed. E. Martín, (ASP, San Francisco), IAU Symposium 211, 325
Allard, F., Hauschildt, P. H., Alexander, D. R., & Starrfield, S. 1997, ARA&A, 35, 137
Allard, F., Hauschildt, P. H., Miller, S., & Tennyson, J. 1994, ApJ, 426, L39
Allard, F., Hauschildt, P. H., & Schwenke, D. 2000, ApJ, 540, 1005
Allard, F., Homeier, D., & Freytag, B. 2012, Phil. Trans. R. Soc. A 370, 2765
Asplund, M., Grevesse, N., Sauval, A. J., & Scott, P. 2009, ARA&A, 47, 481

Baraffe, I., Chabrier, G., Allard, F., & Hauschildt, P. H. 1998, A&A, 337, 403
Burgasser, A. J., et al. 2002, ApJ, 571, L151
Burrows, A., Sudarsky, D., & Hubeny, I. 2006, ApJ, 640, 1063
Caffau, E., et al. 2011, Sol. Phys., 268, 255
Casagrande, L., Flynn, C., & Bessell, M. 2008, MNRAS, 389, 585
Castelli, F., & Kurucz, R. L. 2004, A&A, 419, 725
Chabrier, G. 2003, PASP, 115, 763
Chabrier, G. 2005, in The Initial Mass Function 50 Years Later, eds. E. Corbelli, F. Palla, & H. Zinnecker, (Springer, Dordrecht), ASSL, 327, 41
Chabrier, G., & Baraffe, I. 1997, A&A, 327, 1039
Chabrier, G., & Baraffe, I. 2000, ARA&A, 38, 337
Dupuy, T. J,. & Liu, M. C. 2012, ApJS, 201, 19
Freytag, B., et al. 2010, A&A, 513, A19
Gaidos, E., Krot, A. N., & Huss, G. R. 2009, ApJ, 705, L163
Golimowski, D. A., et al. 2004, AJ, 127, 3516
Grevesse, N., Asplund, M., & Sauval, A. J. 2007, Space Sci. Rev., 130, 105
Grevesse, N., Noels, A., & Sauval, A. J. 1993, A&A, 271, 587
Gustafsson, B., et al. 2008, A&A, 486, 951
Hauschildt, P. H., Allard, F., & Baron, E. 1999, ApJ, 512, 377
Helling, C., et al. 2008a, MNRAS, 391, 1854
Helling, C., Dehn, M., Woitke, P., & Hauschildt, P. H. 2008b, ApJ, 675, L105
Huang, X., Schwenke, D. W., & Lee, T. J. 2011a, J. Chem. Phys., 134, 044320
Huang, X., Schwenke, D. W., & Lee, T. J. 2011b, J. Chem. Phys., 134, 044321
Kasting, J. F. 2001, AGU Fall Meeting Abstracts, C1
Kippenhahn, R., & Weigert, A. 1994, Stellar Structure and Evolution, (Springer, Berlin)
Landau, L. D., & Lifshitz, E. M. 1960, Course of Theoretical Physics, Electrodynamics of Continuous Media, (Pergamon Press, Oxford)
Lodders, K., & Fegley, Jr., B. 2006, in Astrophysics Update 2, ed. Mason, J. W., (Springer, Berlin), 1
Ludwig, H. G., Allard, F., & Hauschildt, P. H. 2002, A&A, 395, 99
Ludwig, H. G., Allard, F., & Hauschildt, P. H. 2006, A&A, 459, 599
Ludwig, H. G., Freytag, B., & Steffen, M. 1999, A&A, 346, 111
Marley, M. S., Saumon, D., & Goldblatt, C. 2010, ApJ, 723, L117
Marois, C., et al. 2008, Science, 322, 1348
Morley, C. V., et al. 2012, ApJ, 756, 172
Paillet, J., Selsis, F., & Allard, F. 2005, in Protostars and Planets V, LPI Contribution No. 1286., p.8341
Rajpurohit, A. S., et al. 2012, A&A, 545, A85
Rajpurohit, A. S., et al. 2013, A&A, 556, 15
Saumon, D., & Marley, M. S. 2008, ApJ, 689, 1327
Seelmann, A. M., Hauschildt, P. H., & Baron, E. 2010, A&A, 522, A102
Tsuji, T. 2002, ApJ, 575, 264
Tsuji, T., Nakajima, T., & Yanagisawa, K. 2004, ApJ, 607, 511
Tsuji, T., Ohnaka, K., & Aoki, W. 1996, A&A, 305, L1
Vrba, F. J., et al. 2004, AJ, 127, 2948
Witte, S., Helling, Ch., & Hauschildt, P. H. 2009, A&A, 506, 1367
Yurchenko, S. N., Barber, R. J., & Tennyson, J. 2011, MNRAS, 413, 1828